Published in final edited form as:
Neuron. 2002 November 14; 36(4): 703–712.

Connexin36 Is Essential for Transmission of Rod-Mediated Visual Signals in the Mammalian Retina

Michael R. Deans[1,5], **Bela Volgyi**[3,5], **Daniel A. Goodenough**[2], **Stewart A. Bloomfield**[3], and **David L. Paul**[1,4]

[1]Department of Neurobiology

[2] Department of Cell Biology Harvard Medical School 200 Longwood Avenue Boston, Massachusetts 02115

[3] Departments of Ophthalmology and Physiology & Neuroscience New York University School of Medicine 550 First Avenue New York, New York 10016

Summary

To examine the functions of electrical synapses in the transmission of signals from rod photoreceptors to ganglion cells, we generated connexin36 knockout mice. Reporter expression indicated that connexin36 was present in multiple retinal neurons including rod photoreceptors, cone bipolar cells, and AII amacrine cells. Disruption of electrical synapses between adjacent AIIs and between AIIs and ON cone bipolars was demonstrated by intracellular injection of Neurobiotin. In addition, extracellular recording in the knockout revealed the complete elimination of rod-mediated, on-center responses at the ganglion cell level. These data represent direct proof that electrical synapses are critical for the propagation of rod signals across the mammalian retina, and they demonstrate the existence of multiple rod pathways, each of which is dependent on electrical synapses.

Introduction

The existence of multiple pathways for transmission of rod signals to the inner retina is supported by studies of retinal anatomy, electrophysiology, and psychophysics (Sharpe and Stockman, 1999; Bloomfield and Dacheux, 2001). In what is widely accepted as the primary rod pathway in the mammalian retina, rod photoreceptors synapse onto rod bipolar cells (RBC) that depolarize in response to light and thus only encode information regarding the onset and duration of the stimulus (Figure 1A). RBCs synapse onto AII amacrine cells, which in turn form inhibitory glycinergic synapses with off-center cone bipolar (OFF CB) terminals and excitatory electrical synapses, in the form of gap junctions, with on-center cone bipolar (ON CB) terminals. In this way, on- and off-center rod signals are created and distributed to cone circuitry in the IPL before reaching appropriate ganglion cell targets.

A second rod pathway was suggested by studies in which rod stimulation continued to evoke off-responses from a subset of retinal ganglion cells after rod input to RBCs was pharmacologically blocked (DeVries and Baylor, 1995). It was proposed that this alternative pathway employed the gap junctions between rods and cones (Raviola and Gilula, 1973) (Figure 1B). In this model, rod excitation would be communicated directly to cone pedicles and then relayed to a subset of ganglion cells via cone bipolar cell circuitry (Smith et al.,

[4] Correspondence: dpaul@hms.harvard.edu.
[5]These authors contributed equally to this work.

1986). This notion was contested by a more recent study of genetically altered, coneless mice (Soucy et al., 1998) in which scotopic OFF responses persisted after pharmacological blockade of the primary pathway. To account for this, it was proposed that OFF CBs directly contacted rods as well as cones (Figure 1C), and subsequent morphological studies revealed that OFF CBs contact 5%–20% of rod photoreceptors in the wild-type mouse (Hack et al., 1999; Tsukamoto et al., 2001). The presence of rod-rod gap junctions, which are numerous in the mouse retina, might pool rod responses and increase the sensitivity of this pathway.

It has been difficult to assess the contribution of multiple rod pathways to ON ganglion cell responses because current pharmacological approaches restrict the analysis to OFF signaling (DeVries and Baylor, 1995; Soucy et al., 1998). To overcome this limitation, we used a genetic approach to selectively eliminate gap junctions between retinal neurons. Gap junctions are composed of intercellular channels that span the plasma membranes of adjacent cells, thereby coupling them with a low-resistance electrical pathway. In vertebrates, these channels are composed of connexins (Cx), a family of proteins with at least 20 members (White and Paul, 1999). Although coupling between retinal neurons is common (Vaney, 1997; Xin and Bloomfield, 1997), the identity of the connexins that comprise these neuronal gap junctions has not been established in most cases. It has been shown, however, that Cx36 is associated with processes within the inner and outer plexiform layers (IPL, OPL) (Deans et al., 2001; Feigenspan et al., 2001; Mills et al., 2001), consistent with expression by multiple cell types. The majority of the Cx36 in the IPL colocalizes with dendritic processes of AII amacrines, suggesting that Cx36 contributes to gap junctions between adjacent AII cells (Feigenspan et al., 2001; Mills et al., 2001) and between AII cells and ON CBs (Mills et al., 2001). Thus, Cx36 is likely to be an important component of ON signaling in at least the primary rod pathway.

We generated mice in which the Cx36 coding sequence was replaced with histological reporters (Deans et al., 2001). Analysis of reporter distribution in the retina of heterozygous animals confirmed expression of Cx36 by AII amacrine cells, but also demonstrated expression in at least rod photoreceptors, two kinds of cone bipolar cells, and a small number of cells within the ganglion cell layer. Microinjection of junction-permeant dye revealed the loss of junctional communication between adjacent AII cells and between AII cells and ON CBs in the Cx36 knockout. Furthermore, extracellular recording from ganglion cells in knockout mouse retinas revealed the complete elimination of on-center responses mediated by rod, but not cone, photoreceptors. These data directly prove that electrical synapses provide a critical function in the propagation of rod signals across the mammalian retina.

Results

β-Gal and PLAP Are Expressed in at Least Five Different Retinal Cell Types

To precisely define the types of retinal neurons expressing Cx36, we examined expression of reporters in heterozygous mice from the Cx36 knockout (KO) line (Deans et al., 2001). In these animals, the Cx36 coding sequence is replaced with a bicistronic reporter cassette containing β-galactosidase (β-gal) and human placental alkaline phosphatase (PLAP). β-gal is a cytoplasmic protein and thus preferentially labels neuronal cell bodies. PLAP is myristylated and associates with the plasma membrane, thereby labeling neuronal processes. Together, these markers provide a number of criteria for identification of Cx36-positive neurons.

β-gal was detected in cell bodies within all nuclear layers and in processes extending throughout both plexiform layers (Figure 2A), consistent with earlier reports demonstrating Cx36 protein expression in these areas (Deans et al., 2001; Feigenspan et al., 2001; Mills et al., 2001). β-gal was detected in the outer nuclear layer (ONL) and in processes extending distal to the outer limiting membrane into the region occupied by photoreceptor inner segments. Together, these observations strongly suggest Cx36 expression by rods, which constitute ~97% of all

photoreceptors in the mouse (Jeon et al., 1998). Within the INL, β-gal-positive neurons were present in two distinct layers (Figure 2A). Cells in the outermost layer displayed characteristic bipolar cell morphology, sending processes into both the IPL and OPL. A second layer of β-gal-positive neurons laid amongst the amacrine cell bodies in the proximal INL. In addition, the reporter was evident in a low number of small neuronal cell bodies within the ganglion cell layer (Figure 2B, arrow), and processes in the vitreal IPL (Figure 2B, arrowhead) when we employed a more sensitive, HRP-linked detection system.

PLAP expression was generally consistent with that of β-gal. However, the PLAP reporter was not fully penetrant and thus did not label all neurons within a particular class (Figure 3A). Although PLAP staining was evident in the ONL, individual neurons could not be visualized. Thus, while PLAP staining was consistent with rod photoreceptor expression of Cx36, it could not be used to resolve the possibility of cone expression. In contrast, isolated PLAP-positive neurons in the INL were frequent and could be identified on the basis of their dendritic/axonal morphology. PLAP stained at least two groups of bipolar cells in the INL, whose axons stratified in either the inner two-thirds (sublamina *b*) (Figure 3B) or outer one-third (sublamina *a*) (Figure 3C) of the IPL. The axonal stratification pattern suggests expression by both on- and off-center bipolar cells (Famiglietti and Kolb, 1975). Within the proximal INL, all PLAP-positive neurons were identified as AII amacrine cells based on well-established morphological criteria, including (1) a cell body located at the most vitreal aspect of the INL and immediately adjacent to the IPL, (2) a narrow-field, bistratified dendritic arborization within both IPL sublaminae, and (3) lobular appendages on dendritic endings within the outer one-third of the IPL (Figure 3D).

Reporter Colocalization with Cell-Specific Markers

Although cone bipolar cells can be divided into as many as 11 different morphological classes (Wassle and Boycott, 1991; Euler and Wassle, 1995), there are very few molecular markers for CB subtypes in the mouse retina (Haverkamp and Wassle, 2000). One unique characteristic of certain CBs is that they accumulate glycine despite the absence of a functional glycine transporter (Cohen and Sterling, 1986; Vaney et al., 1998). Therefore, an antibody against glycine was used to mark a subpopulation of CBs. In the heterozygous retina, some β-gal-positive bipolar cells contained glycine (Figure 4A, arrows), whereas others clearly did not (Figure 4A, arrowheads). This finding confirms and extends the suggestion from PLAP labeling (Figures 3A–3C) that Cx36 is present in at least two classes of CB.

The identification of reporter-positive amacrine cells as type AII was confirmed by double immunofluorescence with β-gal and an AII cell marker. Since markers specific for AII cells in other species (calretinin in rabbit; parvalbumin in rat) label different populations of cells in the mouse (Haverkamp and Wassle, 2000), we used the glycine transporter GLYT1. Glycinergic amacrines formed two distinct layers of cells in the vitreal INL. All β-gal-positive neurons in the amacrine cell layer and immediately adjacent to the IPL were also GLYT1 positive (Figure 4D, arrows).

Double labeling ruled out expression in other cell types whose somata lay in the INL. As illustrated in Figures 4B and 4C, β-gal did not colocalize with the Muller glial marker CRALBP (Bunt-Milam and Saari, 1983), or the rod bipolar marker PKCα (Haverkamp and Wassle, 2000). In addition, we showed previously that horizontal cells, identified by calbindin expression, do not express Cx36 (Deans and Paul, 2001).

Junctional Coupling Is Disrupted in the Cx36 KO Retina

We used two independent methods to evaluate junctional coupling in the wild-type (WT) and Cx36 KO retina. The first method was based on the proposal by Cohen and Sterling (Cohen

and Sterling, 1986) that glycine concentrated by glycinergic amacrine cells could diffuse through gap junctions and accumulate to detectable levels in CBs to which they are coupled. In support of this idea, it was found that CB accumulation of glycine was acutely sensitive to the gap junction blocker carbenoxolone (Vaney and Weiler, 2000). If this model is correct, and if AII-CB gap junctions contain Cx36, then glycine should not be detected in CBs in the Cx36 KO. To evaluate this possibility, the distribution of glycine was determined by immunofluorescence in frozen sections of $Cx36^{+/-}$ and KO retinas. Sections were counter-stained for GLYT1 to mark glycinergic amacrine cells (Figures 4E and 4F). In $Cx36^{+/-}$, glycine was evident in both GLYT1-positive cells and a subset of cells in the middle of the INL that are likely bipolar cells (Figure 4E). In contrast, glycine was restricted to glycinergic amacrine cells in the Cx36 KO retina (Figure 4F). Similar observations were made by Guldenagel et al. (2001) and are consistent with the idea that gap junctions between AII amacrine cells and ON CBs are eliminated in the KO.

A more direct method we employed to evaluate gap junctional coupling of AII amacrine cells involved intracellular injection of Neurobiotin, which has been shown to permeate AII gap junctions (Vaney, 1991; Hampson et al., 1992; Mills and Massey, 1995; Bloomfield et al., 1997). This approach allowed us to unambiguously identify the impaled cell by its physiological response to light stimulation prior to injection, and by its characteristic morphological features visualized after histological processing. In the rabbit retina, Neurobiotin injected into individual AII amacrine cells is detectable both in adjacent AII cells and in the overlying ON CBs (Mills and Massey, 1995; Bloomfield and Xin, 1997), consistent with the existence of gap junctions between these cell types. As demonstrated in Figure 5, a similar if not identical pattern of tracer coupling is evident in mouse retina. Figure 5 contains images from two focal planes. Following iontophoretic injection of Neurobiotin into a single AII cell, the tracer diffused into at least 18–20 neighboring AII cells (Figure 5A) as well as a similar number of bipolar cells in the more distal INL (Figure 5B). In the Cx36 KO, however, Neurobiotin was apparent in only two cells, indicating a dramatic reduction in coupling between neighboring AIIs and ON CBs in the Cx36 KO (Figures 5D and 5E). Vertical sections were used to confirm the identities of injected cells (Figures 5C, 5F, and 5G). Thus, the heavily labeled cell in the KO retina (Figure 5F) displays characteristic morphology of an AII amacrine while the lightly labeled cell is neither an AII nor an ON CB (Figure 5G). It is most likely that the lightly labeled cell is not coupled to the injected AII but was nicked by the injection pipette during penetration or withdrawal. These data are representative of four experiments.

Rod Pathways Are Disrupted in the Cx36 KO

Extracellular recordings were obtained from ganglion cells visualized and targeted under infrared illumination. The sampling pool included ganglion cells with a wide range of cell body shapes and sizes. Thus, responses from a large number of subtypes were obtained. These included cells with a wide range of activities in terms of prominence of transient and/or sustained response components, level of spontaneous spike rate, and relative increase in spike rate in response to a given light stimulus. This made it difficult to directly compare the response physiology of individual cells both within and between WT and KO retinas. We therefore focused on one parameter, the normalized spike rate after background subtraction. This allowed us to compare the light-evoked responses of individual dark-adapted on-center ganglion cells at different stimulus intensities.

Examples of responses from an on-center ganglion cell in a WT or Cx36 KO mouse retina to different stimulus intensities are illustrated in Figure 6A. Both cells show a transient burst of spikes at light onset followed by a sustained increase in spiking for the stimulus duration, particularly for brighter lights. However, there is a clear difference in their sensitivities. The WT ganglion cell displays a detectable threshold response to a stimulus intensity of 0.2

Rhodopsin/isomerizations/rod/s (Rh*/rod/s) and a robust transient response at 4.7 Rh*/rod/s. In contrast, responses from the ganglion cell in the KO mouse did not exceed background firing levels until the stimulus intensity was raised to least 62 Rh*/rod/s. The difference in response threshold and sensitivity between on-center ganglion cells exemplified in Figure 6A was found to be a general and important distinction between the cells in WT and Cx36 KO mouse retinas.

Normalized responses of WT and KO ganglion cells were plotted as intensity-response functions in Figures 6B and 6C. Strikingly, we found that each cell in WT retina (n = 63 from 30 retinae) could be grouped into one of four physiologic classes based on these data (Figure 6B). The intensity-response functions of three of these classes were well fit by a Michaelis-Menten function. Using 5% of maximum response as a threshold criterion, the highest sensitivity cells responded to 0.04 Rh*/rod/s, within the theoretical range for rod photoreceptor threshold sensitivity (Barlow et al., 1971). Response from intermediate sensitivity cells initiated at stimulus levels about an order of magnitude higher, and the least sensitive cells showed response thresholds of about 30 Rh*/rod/s. Most high sensitivity ganglion cells continued to respond to brighter lights, but the amplitude of these responses never increased from the maximum, saturated firing rates. In addition, a small number of high sensitivity cells showed a decline in responsiveness (data not shown) to light intensities above 10–100 Rh*/rod/s, suggesting that they may receive input exclusively from rods. It is therefore likely that the high sensitivity group can be further divided, but this issue was beyond the scope of the present study.

The fourth class of ganglion cells had a wide operating range with a biphasic intensity-response relation that could be fit by two separate Michaelis-Menten functions. These cells exhibited a threshold roughly equal to that of the intermediate sensitivity ganglion cells, but were not driven to saturation by scotopic stimuli. We occasionally encountered cells with intensity-response functions that could not be well fit by a Michaelis-Menten function (data not shown). These cells responded sluggishly and inconsistently to the full-field stimuli we used and so their responses were not included in the summary plot (Figure 6B). Therefore, our sample pool is biased toward cells likely falling within the classic brisk rather than the sluggish response category (Levick, 1967; Caldwell and Daw, 1978).

On-center ganglion cells in the Cx36 KO mouse showed intensity-response functions dramatically different from those of cells in the WT retina (Figure 6C). In fact, all the cells (n = 31 from 16 retinas) could be placed into a single class with a threshold at ~30 Rh*/rod/s. Both the shape of this function and the response threshold are similar if not identical to those of the low sensitivity ganglion cell class found in the WT retina. Clearly, ganglion cells falling within the high sensitivity, intermediate sensitivity, and wide operating range classes are missing in the Cx36 KO mouse.

The simplest interpretation of our data is that only cone-mediated on-center signals reach the ganglion cells in the Cx36 KO mouse retina. However, proof requires independent measurement of the cone threshold in the mouse flattened-eyecup preparation we employed. We measured cone threshold by two methods, the first of which relies on the difference in flicker-fusion frequency responses of rods and cones. In preliminary studies, we found that ganglion cell responses to flickering stimuli near rod threshold (0.04 Rh*/rod/s) fused at rates above about 8 Hz. In contrast, ganglion cells followed photopic stimuli flickering at rates up to at least 15 Hz, consistent with published values (Krishna et al., 2002). Accordingly, we used 10 Hz flickering lights as our cone-specific stimulus, and representative responses from an individual ganglion cell in the WT retina are presented in Figure 7A. Although this cell shows spontaneous spiking in response to low intensity stimulus, a rhythmic response to the stimulus was only seen when the intensity level was raised above cone threshold. The emerging 10 Hz peaks in power spectra of response trains from this cell were plotted. Threshold was determined

using 5% of maximum response (Figure 7C, filled circle) and compared to the KO threshold (open square). The mean threshold from eight WT cells was 31.4 Rh*/rod/s ± 1.1 SEM.

In the second method, cone responses were isolated using paired-pulse stimulation in which rod responses were temporarily suppressed using saturating flashes of light (Lyubarsky and Pugh, 1996) (Figures 7D and 7E). Test flashes of varying intensity were presented 500 ms after suppression to elicit cone responses. A test flash of 12.5 Rh*/rod/s (Figure 7D) elicited no change in spike rate relative to baseline. In contrast, the change in spike rate induced by a 129 Rh*rod/s test flash was significant (Figure 7D). The response of this cell to test flashes of increasing intensities is plotted in Figure 7E (WT threshold, filled circle; KO threshold, open square). The mean threshold from ten WT cells was 31.6 Rh*/rod/s ± 1.2 SEM. Thus, cone thresholds measured by both methodologies match the response threshold of the low sensitivity ganglion cells in the WT retinas and the single ganglion cell class found in the KO.

Discussion

We generated a line of KO mice in which the Cx36 coding sequence was replaced with two histological reporters. The “knockin” strategy avoided significant obstacles in identifying the cells expressing Cx36 and revealed its expression in a diverse set of retinal neurons. The KO retina displayed a complete loss of rod-mediated, but not cone-mediated, on-center ganglion cell responses, proving that electrical synapses are required in all rod ON signaling pathways.

The Distribution of Cx36 in the Rod Pathways

In mice heterozygous for the Cx36 deletion, reporter expression could be detected in several cell populations. Our observations are consistent with previous reports localizing Cx36 in AII amacrine cells (Feigenspan et al., 2001; Mills et al., 2001). However, we also found reporter expression in cells with characteristic bipolar cell morphology, including glycine-positive cells whose axons projected to the proximal “on” sublamina in the IPL. Thus, our data strongly suggests that Cx36 is expressed by ON CBs coupled to AII amacrine cells. In contrast, earlier studies did not find Cx36 in dissociated cells with CB morphology or in ON CBs identified by intracellular dye injection in retinal slices (Feigenspan et al., 2001).

The abundance of reporter in the ONL suggests expression of Cx36 in rod photoreceptors, which had not been previously described. We were unable to determine if cones also express these reporters. Gap junctions between rods and cones have been visualized by freeze fracture electron microscopy in the rabbit and macaque (Raviola and Gilula, 1973, 1975). In addition, junctions between rods and cones as well as between adjacent rods have been described in mouse retina (Tsukamoto et al., 2001). Together, these findings are consistent with the presence of reporters in mouse photoreceptors. In addition, rod-cone coupling has been directly measured in cold-blood vertebrates (Schwartz, 1975; Yang and Wu, 1989; Krizaj et al., 1998), and although similar studies are more difficult in mammalian retinae, rod signals within cone responses have been reported in cat (Nelson, 1977) and macaque (Schneeweis and Schnapf, 1995). Together, these data make it likely that Cx36 comprises functional rod-cone gap junctions in the mouse.

Multiple Rod Pathways in the WT Mouse Retina

In the WT mouse retina, on-center ganglion cells could be divided into four groups based upon their intensity-response profiles and response thresholds to full-field illumination. The low sensitivity group displayed threshold characteristics identical to the isolated cone response. Two groups had responses primarily in the scotopic range; one with a very sensitive response close to the theoretical threshold for rods and another with intermediate sensitivity and a threshold about 1 log unit higher. The fourth group had a wide operating range describing a

two-limbed response curve indicative of a transition from rod- to cone-mediated responses (rod-cone break) (Aguilar and Stiles, 1954). However, the scotopic responses of these cells matched those of the intermediate sensitivity group. Taken together, our data suggest two types of rod-mediated on-center signals arriving at the ganglion cell level. This scheme is consistent with psychophysical studies of rod monochromats, suggesting that the two rod pathways operate at different background light intensities (reviewed in Sharpe and Stockman, 1999). How do these two types of rod signals arise? The most parsimonious explanation is that rod signals are transmitted via the two independent pathways: a primary pathway through AII cells and an alternative pathway created by rod-cone coupling (Figures 1A and 1B). It has been assumed from the psychophysical work as well as electrophysiological studies (Smith et al., 1986; Muller et al., 1988; DeVries and Baylor, 1995; Soucy et al., 1998) that the AII pathway conveys the most sensitive rod response. If so, then our data indicate that only a subset of ganglion cells, those in the high sensitivity category, receive rod input through this pathway. It follows then that the remaining scotopic signals are communicated through the alternative pathway to intermediate sensitivity and wide operating range cell types. Loss of intermediate sensitivity responses in the knockout indicate that this pathway also requires Cx36 and suggests that photoreceptor coupling has been disrupted in the knockout retina.

Our data suggest that a substantial number of ganglion cells display only photopic responses. Although initially surprising, this is entirely consistent with previous studies of ganglion cell responses in the dark-adapted mouse retina. In both isolated (Stone and Pinto, 1993) and in vivo (Balkema and Pinto, 1982) retinal preparations, threshold intensities ranged over at least 4 orders of magnitude, suggesting a population of ganglion cells driven solely by cones. However, each mouse cone establishes gap junctions with multiple rods (Tsukamoto et al., 2001), implying that every ganglion cell should receive input from rods through the rod-cone pathway. Thus, we speculate the existence of a mechanism for the suppression of rod responses in a subset of ganglion cells. This issue awaits further study.

A limitation of our genetic model is that ganglion cell sensitivity must be compared in two separate groups of mice, rather than sequentially in an individual mouse as would be possible with pharmacological approaches. Thus, it remains possible that the reduction in sensitivity in the KO is the indirect result of a gross developmental change in rod circuitry, i.e., cell loss or miswiring. However, comparison of marker distribution in $Cx36^{+/-}$ and KO animals suggested no loss of Cx36-expressing cells. In addition, there was no difference in the percentage of choline acetyl transferase (CAT)-positive cells in the ganglion cell layer between WT and KO retina (WT = 13.1% ± 0.9% SEM CAT-positive cells; KO = 13.4% ± 0.8% SEM CAT-positive cells), indicating no change in total number of ganglion cells. Furthermore, intrinsic rod photoreceptor responses are normal as assayed by ERG (Laura Frishman, personal communication). Finally, if the retina were miswired, then scotopic OFF as well as ON responses should be eliminated or substantively altered. However, we continued to record robust scotopic OFF responses from ganglion cells (data not shown). The contributions of multiple rod pathways in off-signaling will be explored in future studies of the Cx36 KO retina.

Experimental Procedures

Immunofluorescence and Immunohistochemistry

Adult WT, KO, or $Cx36^{+/-}$ mice (all C57BL6/129SvEv hybrids) were deeply anesthetized with an IP injection of Rompun/Ketaset (10–50 mg/ml) and were perfused with 4% paraformaldehyde/Sorenson's buffer (pH 7.4). Eyes were removed and post-fixed for 2 hr as an eye-cup and thoroughly washed in PBS. Tissues were cryoprotected overnight in 20% sucrose and 14–20 μm frozen sections were prepared and mounted onto Superfrost Plus™ microscope slides (Fisher). Slides were washed thoroughly in PBS, blocked with 10% donkey serum, 2% BSA and incubated overnight with primary antibodies, and 2–3 hr with Cy2 (diluted

1:250) or Cy3 (diluted 1:500) labeled secondary antibodies (Jackson ImmunoResearch, West Grove, Pennsylvania). Rabbit anti-β-gal antisera (Chemicon, Temecula, California) was pre-absorbed to WT mouse brain homogenates to reduce nonspecific labeling. Horseradish peroxidase immunohistochemistry was performed using the ABC Elite™ staining kit (Vector, Burlingame, California) according to the manufacturer's directions. Rabbit polyclonal antisera for β-gal (diluted 1:2500) and goat polyclonal antisera for GLYT-1 (diluted 1:2500) were purchased from Chemicon. However, we used a mouse monoclonal β-gal antibody (diluted 1:50; Sigma, St. Louis Missouri) for colocalization experiments with CRALBP. Rabbit anti-CRALBP (diluted 1:5000) was a gift from John C. Saari, and rat anti-glycine (diluted 1:2500) was a gift from David Pow. Mouse monoclonal clone MC5 for PKCα (diluted 1:500) was purchased from Sigma.

To assess ganglion cell number, whole-mount WT (n = 3) and KO (n = 3) retinas were prepared as described above and stained with DAPI to visualize nuclei and for choline acetyl transferase (CAT) using antibodies (Chemicon) to control for eccentricity (Jeon et al., 1998). Micrographs of the ganglion cell layer were taken and cells (~500/field) were counted in 3–4 fields from each retina.

PLAP Histochemistry

Mice were anesthetized and perfused as described above using 2% paraformaldehyde, 1% glutaraldehyde/Sorenson's Buffer (pH 7.4). Eyecups were post-fixed for 2 hr at 4°C, washed thoroughly with PBS, and placed at 65°C for 30 min to denature endogenous phosphatases. Tissue was then cryoprotected overnight with 20% sucrose in Sorenson's (pH 7.4) and frozen in OCT with liquefied propane. Frozen sections were cut at 20 μm and rinsed 3 × 5 min in PLAP reaction buffer (100 mM Tris [pH 9.5], 100 mM NaCl, 50 mM $MgCl_2$, 1% Tween20), and reacted in the same supplemented with 250 μg/ml NitroBlue Tetrazolium and 125 μg/ml 5-bromo-4-chloro-3-indolyl-phosphate in the dark and at room temperature for 4 to 20 hr.

Electrical Recordings

$P_{42\text{-}90}$ wild-type and Cx36 KO mice were used for single unit extracellular recordings. The animals were deeply anesthetized with an intra-peritoneal injection of Nembutal (0.08 g/g body weight), and lidocaine hydrochloride (20 mg/ml) was applied locally to the eyelids. A flattened retinal-scleral preparation developed for rabbit by Hu et al. (2000) was adopted and modified for mouse. Briefly, the eye was removed under dim red illumination and hemisected 1–3 mm anterior to the ora serrata. The lens was removed and the resultant eyecup preparation was placed in a superfusion chamber. Several radial incisions were made peripherally and the retina was flattened in the chamber with the ganglion cell side facing up. After removal of the vitreous humor, the chamber was mounted in a light-tight Faraday-cage and superfused with oxygenated mammalian Ringer solution (pH 7.4, 32°C; Bloomfield and Miller, 1982).

Eyecups were then dark adapted for 1 hr. Extracellular recordings were obtained from ganglion cells using insulated tungsten micro-electrodes (resistance 0.9–1.2 MΩ; Micro Probe, Inc. Potomac, Maryland). Extracellular trains of spikes were recorded digitally at a sampling rate of 20 kHz with Axoscope 8.0.3.168 (Axon Instruments, Inc. Foster City, California). For further off-line analysis, Off-line Sorter 1.39 (Plexon Inc. Dallas, Texas) and Nex 2.653 (Nex Technologies, Littleton, Massachusetts) were used. Datapoints were fitted by the classic Michaelis-Menten equation (cf. Baylor et al., 1974; Naka and Rushton, 1966; Thibos and Werblin, 1978).

$$R=\frac{R_{\max}I^a}{I^a+\sigma^a}$$

where R = measured response, R_{max} = maximum response, I = stimulus intensity, σ = light intensity that produces response of 0.5 R_{max}, and a = Hill coefficient (Microcal Origin 6.0 Microcal Software, Inc. Northampton, Massachusetts).

A green (λ = 468 nm) LED light source was used to deliver uniform full-field visual stimuli to the surface of the retina. The intensity of the square wave light stimuli was calibrated with a portable radiometer/photometer (Ealing Electro-Optics, Inc. Holliston, Massachusetts) and expressed in terms of the time-averaged rate of photoisomerizations per rod (Rh*/rod/s). Light intensities were calculated assuming an average rod density of 437,000 rods/mm^2 (Jeon et al., 1998) and quantum efficiency of 0.67 (Penn and Williams, 1984). The light stimuli intensities varied from 10^{-4}–10^4 Rh*/rod/s.

Neurobiotin Labeling and Histology

Intracellular tracer injections of AII amacrine cells were obtained with standard borosilicate glass microelectrodes (Sutter Instrument Co. Novato, California). Electrodes were filled at their tips with 4% N-(2-amino-ethyl)-biotinamide hydrochloride (Neurobiotin, Vector Laboratories, Burlingame, California), in 0.1 M Tris buffer (pH 7.6) and then back filled with 4 M potassium chloride. Neurobiotin was iontophoresed into the neurons using a sinusoidal (3 Hz, 0.8 nA peak-to-peak) current for 10–15 min. One hour after the labeling of the last cell, the retina was fixed in a cold (4°C) solution of 4% paraformaldehyde in 0.1 M phosphate buffer (pH 7.3) overnight. Retinas were then washed in phosphate buffer and soaked in a solution of 0.18% hydrogen peroxide in methyl alcohol for an hour. This treatment completely abolished the endogen peroxidase activity. Retinas were then washed in phosphate buffer and reacted with the Elite ABC kit (Vector Laboratories, Burlingame, California) and 1% Triton X-100 in 10 nM sodium phosphate-buffered saline (9% saline, pH 7.6). Retinas were subsequently processed for peroxidase histochemistry using 3,3′-diaminobenzidine (DAB) using cobalt for intensification. Retinas were then dehydrated and flat-mounted or sectioned for light microscopy.

Acknowledgments

We are grateful for the superb technical assistance of Marta Mastroianni and Maggie Vanderberg in managing the animal colonies. This study was supported by an Ilfeld Foundation award to D.L.P., National Institutes of Health grants GM37751 to D.L.P, GM18974 to D.A.G., EY07360 to S.A.B., a Fight-for-Sight Postdoctoral Fellowship to B.V. from Prevent Blindness America, Inc., and NIH P30-HD18655 to MRRC at Children's Hospital, Boston.

References

Aguilar M, Stiles WS. Saturation of the rod mechanism of the retina at high levels of stimulation. Opt. Acta (Lond.) 1954;1:59–65.

Balkema GW Jr. Pinto LH. Electrophysiology of retinal ganglion cells in the mouse: a study of a normally pigmented mouse and a congenic hypopigmentation mutant, pearl. J. Neurophysiol 1982;48:968–980. [PubMed: 7143036]

Barlow HB, Levick WR, Yoon M. Responses to single quanta of light in retinal ganglion cells of the cat. Vision Res. Suppl 1971;3:87–101.

Baylor DA, Hodgkin AL, Lamb TD. The electrical response of turtle cones to flashes and steps of light. J. Physiol 1974;242:685–727. [PubMed: 4449052]

Bloomfield SA, Dacheux RF. Rod vision: pathways and processing in the mammalian retina. Prog. Retin. Eye Res 2001;20:351–384. [PubMed: 11286897]

Bloomfield SA, Miller RF. A physiological and morphological study of the horizontal cell types of the rabbit retina. J. Comp. Neurol 1982;208:288–303. [PubMed: 6288777]

Bloomfield SA, Xin D. A comparison of receptive-field and tracer-coupling size of amacrine and ganglion cells in the rabbit retina. Vis. Neurosci 1997;14:1153–1165. [PubMed: 9447695]

Bloomfield SA, Xin D, Osborne T. Light-induced modulation of coupling between AII amacrine cells in the rabbit retina. Vis. Neurosci 1997;14:565–576. [PubMed: 9194323]

Bunt-Milam AH, Saari JC. Immunocytochemical localization of two retinoid-binding proteins in vertebrate retina. J. Cell Biol 1983;97:703–712. [PubMed: 6350319]

Caldwell JH, Daw NW. New properties of rabbit retinal ganglion cells. J. Physiol 1978;276:257–276. [PubMed: 650447]

Cohen E, Sterling P. Accumulation of (3H)glycine by cone bipolar neurons in the cat retina. J. Comp. Neurol 1986;250:1–7. [PubMed: 3734165]

Deans MR, Paul DL. Mouse horizontal cells do not express connexin26 or connexin36. Cell Adhes. Commun 2001;8:361–366.

Deans MR, Gibson JR, Sellitto C, Connors BW, Paul DL. Synchronous activity of inhibitory networks in neocortex requires electrical synapses containing connexin36. Neuron 2001;31:477–485. [PubMed: 11516403]

DeVries SH, Baylor DA. An alternative pathway for signal flow from rod photoreceptors to ganglion cells in mammalian retina. Proc. Natl. Acad. Sci. USA 1995;92:10658–10662. [PubMed: 7479860]

Euler T, Wassle H. Immunocytochemical identification of cone bipolar cells in the rat retina. J. Comp. Neurol 1995;361:461–478. [PubMed: 8550893]

Famiglietti EV Jr. Kolb H. A bistratified amacrine cell and synaptic circuitry in the inner plexiform layer of the retina. Brain Res 1975;84:293–300. [PubMed: 1111833]

Feigenspan A, Teubner B, Willecke K, Weiler R. Expression of neuronal connexin36 in AII amacrine cells of the mammalian retina. J. Neurosci 2001;21:230–239. [PubMed: 11150340]

Guldenagel M, Ammermuller J, Feigenspan A, Teubner B, Degen J, Sohl G, Willecke K, Weiler R. Visual transmission deficits in mice with targeted disruption of the gap junction gene connexin36. J. Neurosci 2001;21:6036–6044. [PubMed: 11487627]

Hack I, Peichl L, Brandstatter JH. An alternative pathway for rod signals in the rodent retina: rod photoreceptors, cone bipolar cells, and the localization of glutamate receptors. Proc. Natl. Acad. Sci. USA 1999;96:14130–14135. [PubMed: 10570210]

Hampson EC, Vaney DI, Wieler R. Dopaminergic moculation of gap junction permeability between amacrine cells in mammalian retina. J. Neurosci 1992;12:4911–4922. [PubMed: 1281499]

Haverkamp S, Wassle H. Immunocytochemical analysis of the mouse retina. J. Comp. Neurol 2000;424:1–23. [PubMed: 10888735]

Hu EH, Dacheux RF, Bloomfield SA. A flattened retina-eyecup preparation suitable for electrophysiological studies of neurons visualized with trans-scleral infrared illumination. J. Neurosci. Methods 2000;103:209–216. [PubMed: 11084214]

Jeon CJ, Strettoi E, Masland RH. The major cell populations of the mouse retina. J. Neurosci 1998;18:8936–8946. [PubMed: 9786999]

Krishna VR, Alexander KR, Peachey NS. Temporal properties of the mouse cone electroretinogram. J. Neurophysiol 2002;87:42–48. [PubMed: 11784728]

Krizaj D, Gabriel R, Owen WG, Witkovsky P. Dopamine D2 receptor-mediated modulation of rod-cone coupling in the Xenopus retina. J. Comp. Neurol 1998;398:529–538. [PubMed: 9717707]

Levick WR. Receptive fields and trigger features of ganglion cells in the visual streak of the rabbits retina. J. Physiol 1967;188:285–307. [PubMed: 6032202]

Lyubarsky AL, Pugh EN Jr. Recovery phase of the murine rod photoresponse reconstructed from electroretinographic recordings. J. Neurosci 1996;16:563–571. [PubMed: 8551340]

Mills SL, Massey SC. Differential properties of two gap junctional pathways made by AII amacrine cells. Nature (Lond.) 1995;377:734–737. [PubMed: 7477263]

Mills SL, O'Brien JJ, Li W, O'Brien J, Massey SC. Rod pathways in the mammalian retina use connexin 36. J. Comp. Neurol 2001;436:336–350. [PubMed: 11438934]

Muller F, Wassle H, Voigt T. Pharmacological modulation of the rod pathway in the cat retina. J. Neurophysiol 1988;59:1657–1672. [PubMed: 3404200]

Naka KI, Rushton WA. An attempt to analyse colour reception by electrophysiology. J. Physiol 1966;185:556–586. [PubMed: 5918059]

Nelson R. Cat cones have rod input: a comparison of the response properties of cones and horizontal cell bodies in the retina of the cat. J. Comp. Neurol 1977;172:109–135. [PubMed: 838876]

Penn JS, Williams TP. A new microspectrophotometric method for measuring absorbance of rat photoreceptors. Vision Res 1984;24:1673–1676. [PubMed: 6533992]

Raviola E, Gilula NB. Gap junctions between photoreceptor cells in the vertebrate retina. Proc. Natl. Acad. Sci. USA 1973;70:1677–1681. [PubMed: 4198274]

Raviola E, Gilula NB. Intramembrane organization of specialized contacts in the outer plexiform layer of the retina. A freeze-fracture study in monkeys and rabbits. J. Cell Biol 1975;65:192–222. [PubMed: 1127010]

Schneeweis DM, Schnapf JL. Photovoltage of rods and cones in the macaque retina. Science 1995;268:1053–1056. [PubMed: 7754386]

Schwartz EA. Cones excite rods in the retina of the turtle. J. Physiol 1975;246:639–651. [PubMed: 1133790]

Sharpe LT, Stockman A. Rod pathways: the importance of seeing nothing. Trends Neurosci 1999;22:497–504. [PubMed: 10529817]

Smith RG, Freed MA, Sterling P. Microcircuitry of the dark-adapted cat retina: functional architecture of the rod-cone network. J. Neurosci 1986;6:3505–3517. [PubMed: 3794785]

Soucy E, Wang Y, Nirenberg S, Nathans J, Meister M. A novel signaling pathway from rod photoreceptors to ganglion cells in mammalian retina. Neuron 1998;21:481–493. [PubMed: 9768836]

Stone C, Pinto LH. Response properties of ganglion cells in the isolated mouse retina. Vis. Neurosci 1993;10:31–39. [PubMed: 8424927]

Thibos LN, Werblin FS. The properties of surround antagonism elicited by spinning windmill patterns in the mudpuppy retina. J. Physiol 1978;278:101–116. [PubMed: 671274]

Tsukamoto Y, Morigiwa K, Ueda M, Sterling P. Microcircuits for night vision in mouse retina. J. Neurosci 2001;21:8616–8623. [PubMed: 11606649]

Vaney DI. Many diverse types of retinal neurons show tracer coupling when injected with biocytin or Neurobiotin. Neurosci. Lett 1991;125:187–190. [PubMed: 1715532]

Vaney D. Neuronal coupling in rod-signal pathways of the retina. Invest. Ophthalmol. Vis. Sci 1997;38:267–273. [PubMed: 9040458]

Vaney DI, Weiler R. Gap junctions in the eye: evidence for heteromeric, heterotypic and mixed-homotypic interactions. Brain Res. Brain Res. Rev 2000;32:115–120. [PubMed: 10751660]

Vaney DI, Nelson JC, Pow DV. Neurotransmitter coupling through gap junctions in the retina. J. Neurosci 1998;18:10594–10602. [PubMed: 9852595]

Wassle H, Boycott BB. Functional architecture of the mammalian retina. Physiol. Rev 1991;71:447–480. [PubMed: 2006220]

White TW, Paul DL. Genetic diseases and gene knockouts reveal diverse connexin functions. Annu. Rev. Physiol 1999;61:283–310. [PubMed: 10099690]

Xin D, Bloomfield SA. Tracer coupling pattern of amacrine and ganglion cells in the rabbit retina. J. Comp. Neurol 1997;383:512–528. [PubMed: 9208996]

Yang XL, Wu SM. Modulation of rod-cone coupling by light. Science 1989;244:352–354. [PubMed: 2711185]

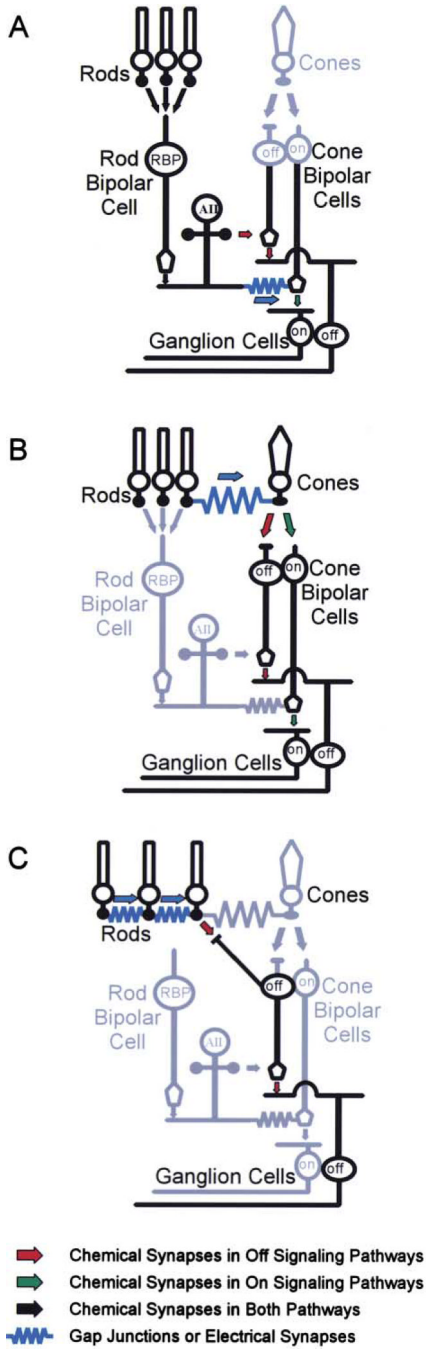

Figure 1. Rod Pathways in the Mouse Retina Utilize Cone Circuitry

(A) In the primary rod pathway, rods synapse onto a single class of rod bipolar cell, which synapses onto the AII amacrine cell. The AII generates parallel streams of ON and OFF by forming excitatory electrical synapses with ON CBs and inhibitory glycinergic synapses with OFF CBs, respectively.

(B) In an alternative rod pathway, rods and cones are directly coupled via electrical synapses, allowing rod excitation to be communicated to ON and OFF CBs via synapses in the cone pedicle.

(C) A third pathway may function in the transmission of OFF information. In this path, rods make flat synapses onto a specialized bipolar cell type that synapses directly onto Off-center ganglion cells.

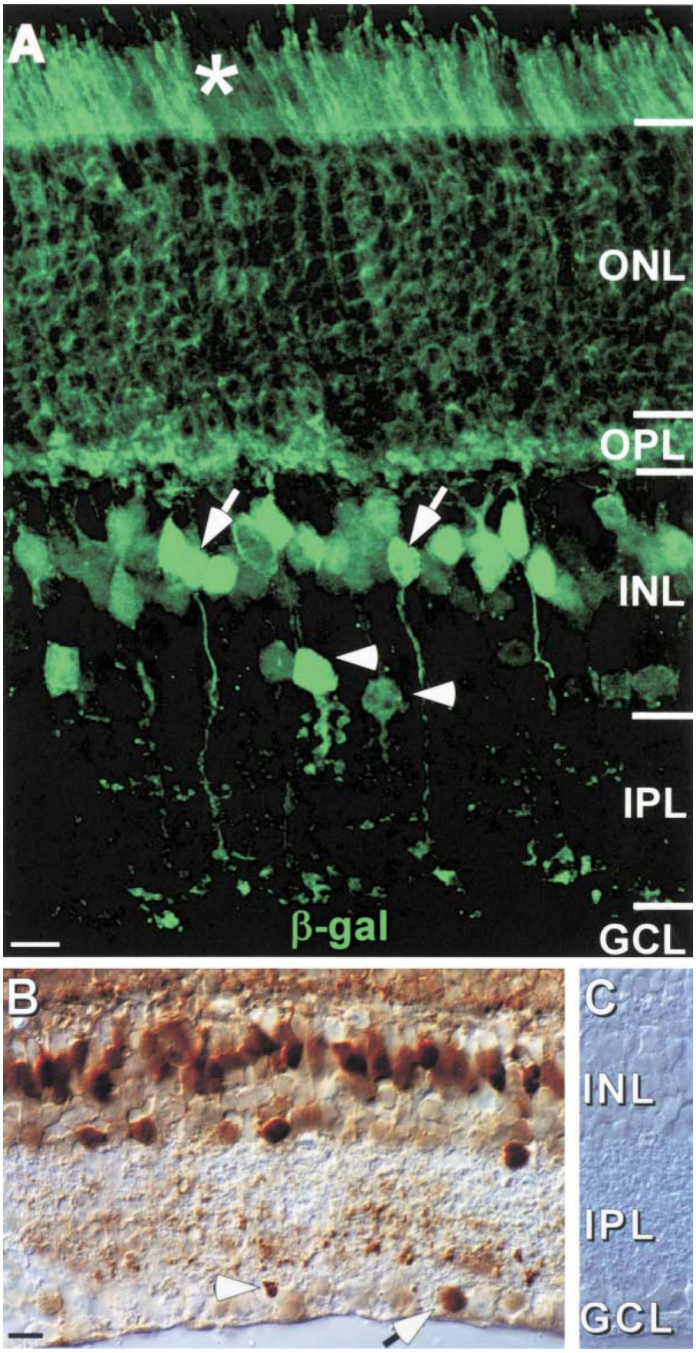

Figure 2. β-Gal Reporter Is Present in the ONL, Amacrine, and Bipolar Cell Layers of the INL and Some Small Cells in the GCL

(A) β-gal immunofluorescence visualized by confocal microscopy can be detected throughout the ONL, and the reporter distinctively labels the photoreceptor inner segments (asterisk). Furthermore, in the INL, β-gal labels cells with characteristic bipolar cell morphology (examples indicated with arrows) and amacrine cells immediately adjacent to the IPL (examples indicated with arrowheads).

(B) β-gal immunohistochemistry detects the reporter in a limited number of neurons with small cell bodies in the GCL that may be displaced amacrine cells (arrow), and also in processes from the IPL immediately adjacent to the GCL (arrowhead).

(C) No reporter can be detected by immunohistochemistry in WT retina. Scale bar equals 10 μm.

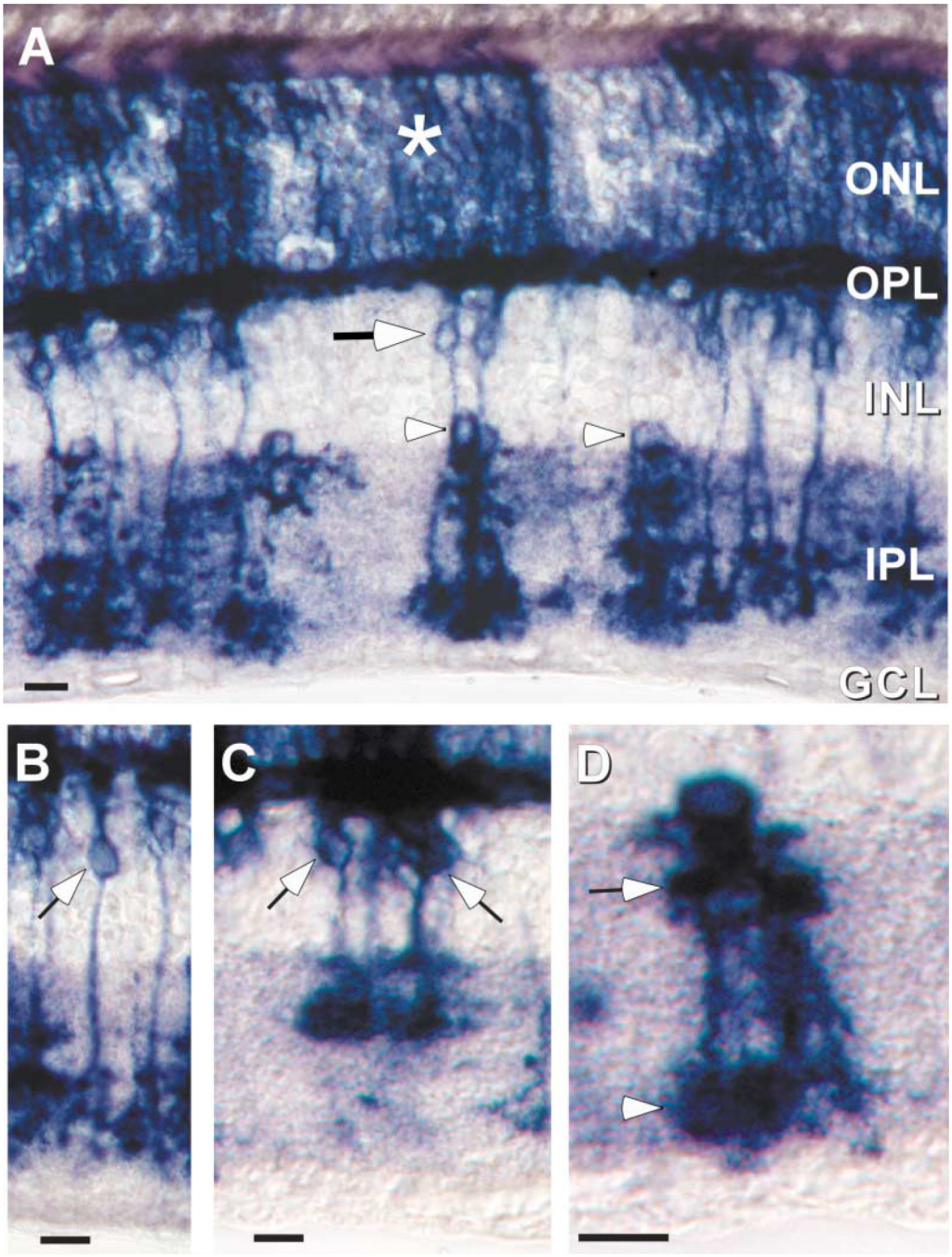

Figure 3. PLAP Reporter Allows Identification of Individual Retinal Neurons

(A) Similar to the distribution of β-gal, PLAP histochemistry labels neurons in the ONL (asterisk), neurons in the bipolar cell layer (arrows), as well as narrow-field and bistratified amacrine cells (arrowheads).

(B and C) PLAP-positive cells in the bipolar cell layer extend processes into the OPL and also into the On (C) and Off (D) layers of the IPL, indicating Cx36 expression by at least two classes of bipolar cell.

(D) Individual PLAP-positive amacrine cells have the morphological characteristics of type AII amacrine cells.

Scale bars equal 10 μm.

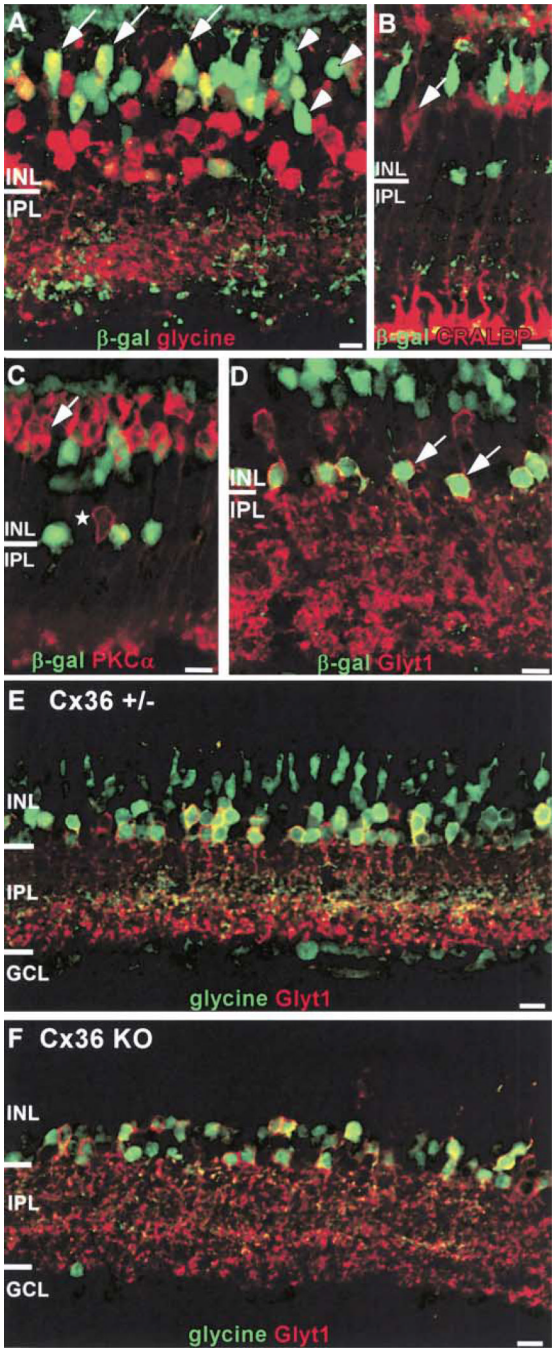

Figure 4. Identification of β-Gal-Positive Neurons in the INL

(A) Some β-gal-positive bipolar cells colocalize with glycine, indicating Cx36 expression in On CBs (examples indicated with arrows). However, β-gal-positive bipolar cells without glycine indicate Cx36 expression by another type of CB (examples indicated by arrowheads). (B and C) Muller glia and rod bipolar cells do not express β-gal. β-gal-positive neurons in the bipolar cell layer do not colocalize with the Muller glia marker CRALBP or the RBC marker PKCα. PKCα also labels a small number of amacrine cells (star) that do not overlap with the β-gal-positive amacrine cells.

(D) In $Cx36^{+/-}$ mice, β-gal-positive amacrine cells located at the most vitreal edge of the INL also colocalize with GLYT1 (examples indicated with arrows), confirming the identification of these cells as AII amacrines.
(E and F) Glycine is readily detected in +/– (E) but not KO (F) bipolar cells, suggesting that the gap junctions between AII amacrines and On CBs require Cx36. Sections were counterstained for GLYT1 to mark glycinergic amacrines..
Scale bars equal 10 μm.

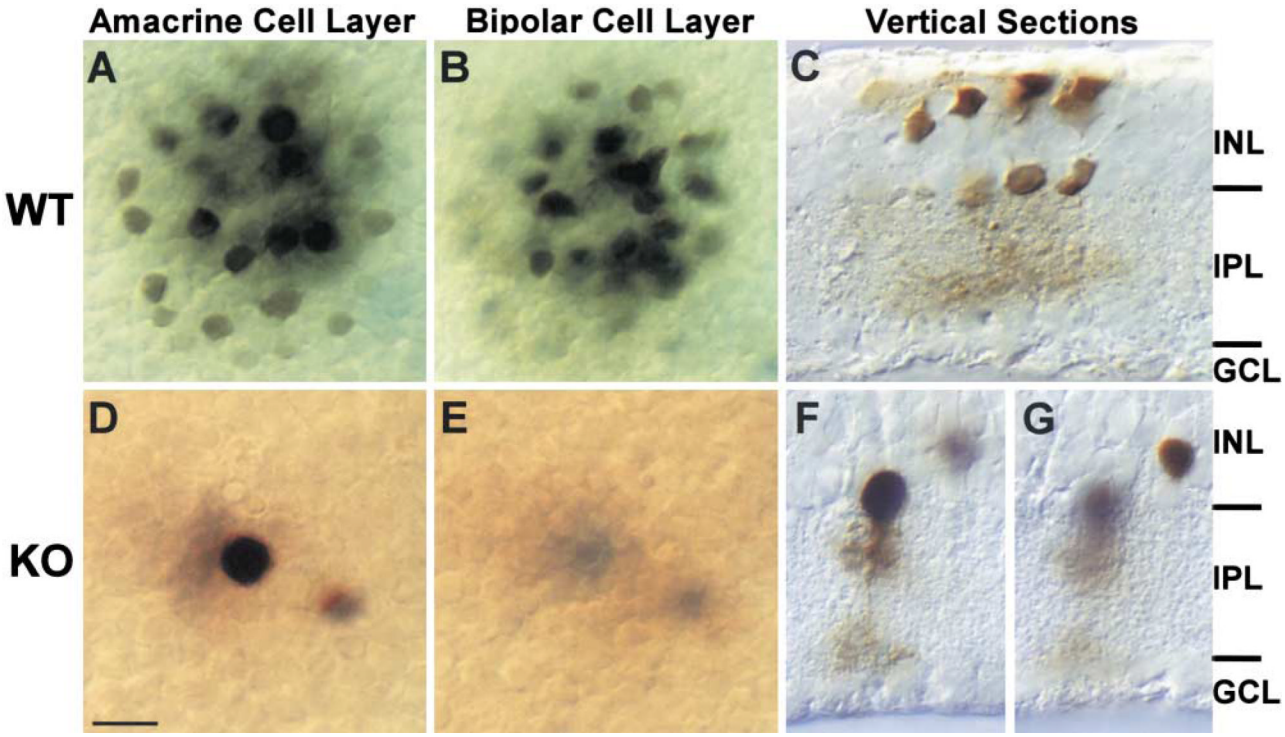

Figure 5. Gap Junctions between AIIs and AII and On CBs Are Disrupted

(A and B) In WT mouse retina, neurobiotin (mw = 284 Da) injected into individual AII amacrine cells is detectable both in adjacent AIIs (A) and in the overlying CBs (B), consistent with the notion that gap junctions couple these cell types.

(D and E) In dramatic contrast, neurobiotin is completely restricted to the injected AII in the Cx36 KO.

(C, F, and G) Vertical sections were used to confirm the identities of injected cells.

Scale bars equal 10 μm.

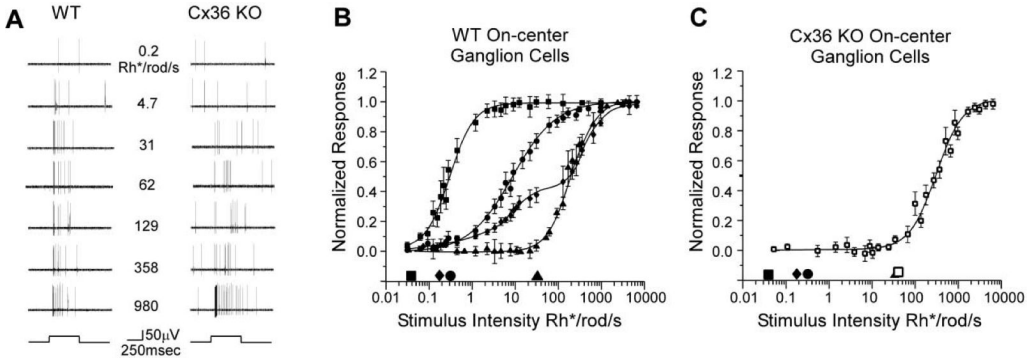

Figure 6. Responses of On-Center Ganglion Cells in WT and Cx36 KO Retina

(A) Representative spike trains recorded extracellularly from on-center ganglion cells in WT (left) and Cx36 KO (right) retina to a 500 ms step of full-field illumination of different intensities. Stimulus onset and offset are indicated by the step functions beneath each row of recordings. Both ganglion cells have similar response components, but KO cell is about 100-fold less sensitive than the WT cell.

(B) Normalized responses of WT on-center ganglion cells as a function of light intensity. Each data point shows the average and standard error for a number of cells. The data were fit by Michaelis-Menten equations as described in the Experimental Procedures. Responses fell into four groups: high sensitivity (squares, n = 18), intermediate sensitivity (circles, n = 30), low sensitivity (triangles, n = 9), and wide operating range (diamonds, n = 6). Symbols along the abscissa indicate the response thresholds for each class of cell using a 5% of maximum response criterion.

(C) Normalized responses of KO on-center ganglion cells as a function of stimulus intensity. All KO on-center ganglion cell had response characteristics similar to WT low sensitivity cells. The open square along the abscissa indicates the threshold of cells in the KO. Symbols indicating the thresholds of WT cell classes are provided for comparison.

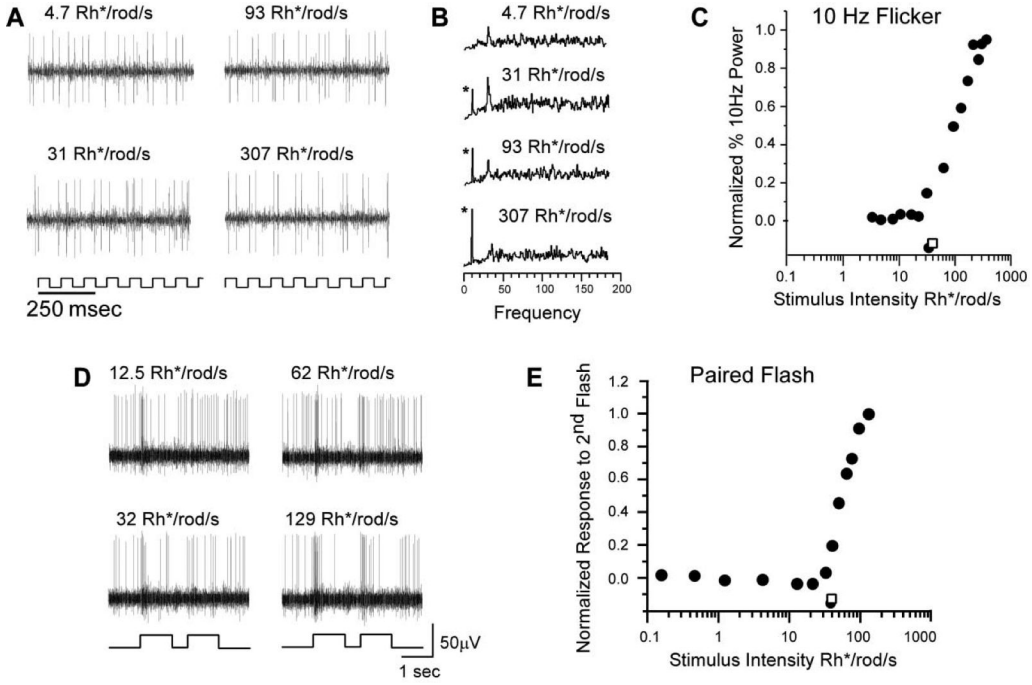

Figure 7. Characterization of the Cone Threshold Using Flickering and Paired-Pulse Light Stimuli

(A) Power spectra for the ganglion cell responses to the 10 Hz flickering light stimuli of increasing light intensity. The response to dim flickering light (4.7 Rh*/rod/s) showed no 10 Hz signal above background noise. The 10 Hz signals are first seen in responses to light at 31 Rh*/rod/s and increases at greater light intensities. Asterisks indicate 10 Hz frequency peaks.

(B) Scatter plot comparison of the normalized 10 Hz signals in the power spectra of the responses to 10 Hz flickering light. As seen in (A), 10 Hz signals are not seen with stimuli less than 31 Rh*/rod/s (WT threshold, filled circle; KO threshold, open square).

(C) Extracellular recordings from a WT on-center ganglion cell. Presentation of the paired-pulse light stimulus is indicated by the light trace beneath each panel of records. The saturating pulse was followed by a pulse of varying intensity as indicated under each trace.

(D) Normalized response of the cell as a function of the intensity of the second flash. The threshold for WT cone photoreceptors was 31.2 Rh*/rod/s (filled circle; KO threshold, open square).